JOURNAL OF SOLID STATE CHEMISTRY **130,** 129–139 (1997)
ARTICLE NO. SC977289

Electronic State, Magnetism, and Electrical Transport Behavior of $Sr_{3-x}A_xFe_2O_7$ ($x \leq 0.4$, $A = Ba, La$)

P. Adler

Max-Planck-Institut für Festkörperforschung, Heisenbergstr. 1, 70569 Stuttgart, Federal Republic of Germany

Received October 29, 1996; accepted January 22, 1997

Tetravalent iron in $Sr_3Fe_2O_7$ reveals a charge disproportionation which is usually formulated as $2Fe^{4+} \rightarrow Fe^{3+} + Fe^{5+}$. With the purpose of studying the influence of valence-conserving and valence-changing cationic substitutions on the electronic properties of this system the phases $Sr_{2.7}Ba_{0.3}Fe_2O_7$ and $Sr_{2.6}La_{0.4}Fe_2O_7$ have been prepared and characterized by several techniques. A sample of $Sr_3Fe_2O_7$ has been studied for comparison. X-ray powder patterns show that the tetragonal crystal structure (space group *I*4/*mmm*) of $Sr_3Fe_2O_7$ is retained in the substituted materials. ^{57}Fe-Mössbauer spectroscopy evidences magnetic ordering effects below 100 K and a charge disproportionation of Fe^{4+} in the magnetically ordered phases of all the compounds. A charge disproportionation of Fe^{4+} is also observed in the paramagnetic phases of $Sr_3Fe_2O_7$ and $Sr_{2.7}Ba_{0.3}Fe_2O_7$, whereas in $Sr_{2.6}La_{0.4}Fe_2O_7$ essentially an average-valence state occurs. Magnetic susceptibility curves of $Sr_3Fe_2O_7$ and $Sr_{2.7}Ba_{0.3}Fe_2O_7$ reveal antiferromagnetic ordering below 100 and 57 K, respectively. A divergence of zero-field-cooled and field-cooled susceptibility data below 50 K indicates the formation of a spin-glass in $Sr_{2.6}La_{0.4}Fe_2O_7$. The magnetic behavior of the compounds is determined by ferro- and anti-ferromagnetic exchange interactions. Electrical resistivity measurements demonstrate that all compounds are semiconductors. The temperature dependence of the conductivities is characterized by a weakly activated low-temperature and a stronger activated high-temperature region. The electronic properties of the title system are interpreted in terms of a collective electronic state which is determined by strong correlation effects associated with the $(\pi^*)^3(\sigma^*)^1$ configuration of Fe^{4+} and a pronounced tendency to delocalize the σ^* electrons arising from the strong covalency of iron–oxygen bonding.

1. INTRODUCTION

Strontium ferrates with iron in the oxidation state +4 form a Ruddlesden–Popper-type series of compounds having the general formula $Sr_{n+1}Fe_nO_{3n+1}$ with $n = 1$ (Sr_2FeO_4 (1)), 2 ($Sr_3Fe_2O_7$ (2, 3)), or ∞ ($SrFeO_3$ (4, 5)). The basic units building up the crystal structures of these compounds are regular or nearly regular FeO_6 octahedra which are connected via common corners to form two-dimensional iron–oxygen layers in the K_2NiF_4-type structure of Sr_2FeO_4 but a three-dimensional network in the cubic perovskite $SrFeO_3$. The crystal structure of $Sr_3Fe_2O_7$, which is isotypic to $Sr_3Ti_2O_7$ (6), is intermediate with respect to the degree of condensation of the FeO_6 octahedra and consists of sheets of Fe_2O_{11} double octahedra. The three compounds are of interest for the study of systematic trends in the electronic properties of transition metal compounds as each of them reveals different electronic behavior.

The Mössbauer spectra of $SrFeO_3$, which is an antiferromagnet ($T_N \approx 130$ K) with a helical spin structure (7), are simple with a single Fe^{4+} site in the paramagnetic phase and the antiferromagnetic phase (8). Stoichiometric $SrFeO_3$ has a nearly temperature-independent conductivity $\sigma \sim 10^3\ \Omega^{-1}\,cm^{-1}$ (5). On the other hand, Sr_2FeO_4 is a semiconductor (9). Its Mössbauer spectra show a single Fe^{4+} site in the paramagnetic phase but a complicated distribution of Fe^{4+} sites in the antiferromagnetic phase ($T_N \approx 60$ K) which has been proposed to arise from structural distortions (9) or from a complicated spin structure (10). Raman spectra of Sr_2FeO_4 reveal an unusual oxygen-derived phonon band, which is not intrinsic to the ideal K_2NiF_4 crystal structure and disappears at pressures above 5 GPa (11). These findings are in favor of a structural instability in Sr_2FeO_4. High-pressure reflectivity studies on Sr_2FeO_4 show an increase in the near-infrared optical reflectivity above 5 GPa, indicating that Sr_2FeO_4 reveals a pressure-driven narrowing of the excitation gap, finally resulting in an insulator–metal transition (11). In fact, metallic temperature dependence of the resistivity at pressures above 18 GPa was reported recently (12).

Mössbauer spectra of the system $Sr_3Fe_2O_{7-\delta}$ were first reported by Gallagher *et al.* (3) who, among others, displayed spectra of a sample with the chemically determined composition $Sr_3Fe_2O_{6.9}$. The spectra were interpreted in terms of Fe^{3+} and Fe^{4+} sites, but the discrepancy between the above composition and the intensity ratio of approximately 1 : 1 for the two sites in the Mössbauer spectra of the magnetically ordered phase was not discussed. Later on, Takano *et al.* suggested that these spectra correspond to

0022-4596/97 $25.00

a charge disproportionation of Fe^{4+} into Fe^{3+} and Fe^{5+} (13). The classic example for this unusual electronic state in oxoferrates(IV) is the tetragonal perovskite $CaFeO_3$ (13). The occurrence of a charge disproportionation of Fe^{4+} in $Sr_3Fe_2O_7$ was confirmed in a recent investigation on a sample where the absence of oxygen deficiency was assured from neutron diffraction data (10). Also in the mixed-valence phases $Sr_{1-x}La_xFeO_3$ (14–16), $Ba_{1-x}La_xFeO_{3-\delta}$ (17), and $Sr_2LaFe_3O_{9-\delta}$ (18) a charge disproportionation of Fe^{4+} has been observed. It is particularly remarkable that there is a continuous change from the $CaFeO_3$- to the $SrFeO_3$-type Mössbauer spectra in the solid solution series $Ca_{1-x}Sr_xFeO_3$ with increasing x (14, 15), which suggests a gradual charge disproportionation according to $2Fe^{4+} \rightarrow 2Fe^{(4-\delta)+} + 2Fe^{(4+\delta)+}$ with nonintegral values for δ in these phases. One might expect that the charge disproportionation is accompanied by a structural distortion arising from the different ionic radii of the two sites which was, however, observed in neither low-temperature neutron diffraction data of $Sr_3Fe_2O_7$ (10) nor those of $Sr_2LaFe_3O_{8.94}$ (19). In the latter case a spin-density wave in the magnetic structure could be established.

As the circumstances which favor the occurrence of a charge disproportionation of Fe^{4+} are poorly understood, it is of interest to investigate the electronic properties of substituted phases in the 3:2:7 system. In the course of attempts to exchange Sr^{2+} in $Sr_3Fe_2O_7$ partly by Ba^{2+} and La^{3+} we have prepared the phases $Sr_{2.7}Ba_{0.3}Fe_2O_7$ and $Sr_{2.6}La_{0.4}Fe_2O_7$. In the first case the iron oxidation state remains +4, whereas in the latter formally 20% Fe^{3+} is introduced. The present contribution reports the synthesis of these materials and their characterization by powder X-ray diffractometry, Mössbauer spectroscopy, magnetic susceptibility, and electrical resistivity measurements. The results are compared with investigations on unsubstituted $Sr_3Fe_2O_7$. In particular, we have investigated the temperature dependence of the Mössbauer spectra of $Sr_3Fe_2O_7$ in more detail than has been reported in the previous studies. The electronic behavior of the strontium ferrates will be discussed in terms of a qualitative Mott–Hubbard picture of the electronic structure.

2. EXPERIMENTAL

Exploratory investigations of the series $Sr_{3-x}A_xFe_2O_{7-\delta}$ for A = Ba and La indicated that single-phase materials can be prepared up to $x \approx 0.4$. The samples used for the present studies were prepared from stoichiometric mixtures of the commercially available oxides Fe_2O_3, SrO, and BaO_2 or La_2O_3 which were ground in a ball mill, heated at 1000°C overnight, pelletized, and heated for another 3 days at 1000°C. The samples were furnace cooled to about 100°C. For reaching high oxygen contents all materials were annealed at oxygen pressures of 60 MPa at 500°C for 18 h in an autoclave. The samples were characterized by X-ray powder diffractometry (STOE powder diffractometer) before and after high-pressure oxygen annealing. For determining accurate lattice constants Si was used as an internal standard.

Room temperature ^{57}Fe-Mössbauer spectra of powdered samples diluted with polyethylene were measured with a conventional Mössbauer spectrometer with a sine-type drive signal. Low-temperature Mössbauer spectra were measured in an Oxford flow cryostat with a Mössbauer spectrometer operating with a triangular drive signal. A $^{57}Co/Rh$ γ-ray source was used for the experiments. The velocity scale was calibrated by measuring the hyperfine splitting of an α-Fe foil. All isomer shifts are referred to α-Fe.

Electrical resistance measurements were performed on high-pressure oxygen annealed pellets of $Sr_{3-x}A_xFe_2O_7$ using the four-point contact method. The resistances R were converted into specific resistivities ρ.

Magnetic susceptibility measurements were performed with a SQUID (Quantum Design or VTS) susceptometer in an external magnetic field of 0.1 T. The samples were first cooled down to 5 K without magnetic field. Subsequently the zero-field-cooled (zfc) curve was obtained by heating to room temperature in the measuring field. A field-cooled (fc) curve was obtained by cooling in the measuring field. The diamagnetic contributions to the magnetic susceptibility were negligible and were not taken into account. The magnetic susceptibilities χ are given in emu mol^{-1}. Multiplying with $4\pi \times 10^{-6}$ leads to the χ values in SI units ($m^3\,mol^{-1}$).

3. RESULTS

The X-ray powder diagrams of $Sr_3Fe_2O_7$ and of the substituted materials $Sr_{2.7}Ba_{0.3}Fe_2O_7$ and $Sr_{2.6}La_{0.4}Fe_2O_7$ reveal only the Bragg reflections expected for the tetragonal space group $I4/mmm$. The lattice constants for the present sample of $Sr_3Fe_2O_7$ and the substituted phases before and after high-pressure oxygen annealing are given in Table 1. High-pressure oxygen annealing leads to a decrease in the

TABLE 1
Lattice Parameters of $Sr_{3-x}A_xFe_2O_7$ Derived from X-Ray Powder Diagrams

		Air-annealed		Annealed at p_{O_2} = 60 MPa	
A	x	a (pm)	c (pm)	a (pm)	c (pm)
	0			385.56(14)	2015.2(5)
Ba	0.3	388.08(3)	2025.8(2)	386.89(5)	2023.6(3)
Ba[a]	0.4	388.76(4)	2029.6(2)	387.16(6)	2025.7(3)
La	0.4	386.86(7)	2021.1(4)	386.15(6)	2019.8(4)

[a] A certain amount of 113 phase is seen in the X-ray diagram.

lattice parameter a. It has been shown by a neutron diffraction study of $Sr_3Fe_2O_{7-\delta}$ (6) that a decreases linearly with increasing oxygen, i.e., with increasing Fe^{4+} content. From the a parameter one derives the composition $Sr_3Fe_2O_{6.94(4)}$ for the present sample. Since oxygen deficiency is small, we restrict for simplicity to the stoichiometric formulation in the case of the high-pressure oxygen annealed samples. For both the Ba- and the La-substituted samples, the lattice parameters a and c are significantly larger than for $Sr_3Fe_2O_7$, which confirms that cationic substitution has taken place. The lattice expansion is more pronounced for the Ba-substituted material. The lattice constants of a sample with a nominal Ba content $x = 0.4$ are still larger than those of the sample with $x = 0.3$ but a small amount of impurity 1:1:3 phase was present in the X-ray diffraction pattern. Attempts to produce materials with higher degrees of substitution have been unsuccessful, so far, in both cases.

Mössbauer spectra of pure $Sr_3Fe_2O_7$ have been collected between 12 and 290 K. In Fig. 1 three representative spectra of the paramagnetic phase are shown; in Fig. 2 spectra of the magnetically ordered phase and of the temperature range of the magnetic phase transition are depicted. The 12- and 290-K spectra are in good agreement with corresponding spectra reported in literature (3, 10).

The spectra of the paramagnetic phase were analyzed by one quadrupole doublet and one single line corresponding to two distinct sites I and II, respectively. Guided by the low-temperature spectra, the intensity ratio between the two sites was fixed to 1:1. The isomer shifts of the two sites are considerably different. It is seen already qualitatively from Fig. 1 that the spectra become more structured with decreasing temperature. In Fig. 3 the temperature dependence of the isomer shifts δ of the two sites, of the difference $\Delta\delta$ in the isomer shifts, and of the quadrupole splitting ΔE_Q of site I are depicted. The temperature dependence of δ is more pronounced for site I than for site II. It is particularly emphasized that both $\Delta\delta$ and ΔE_Q are temperature dependent and increase with decreasing temperature.

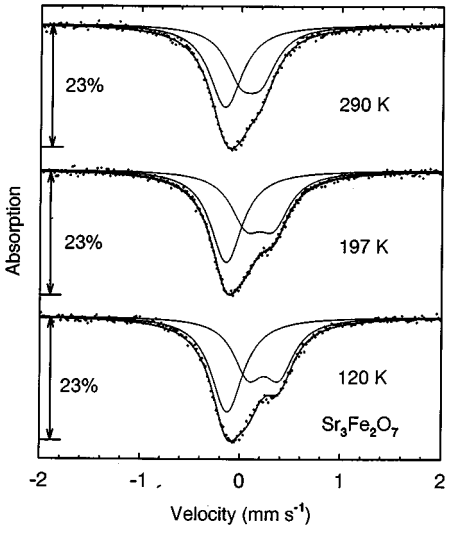

FIG. 1. Mössbauer spectra of $Sr_3Fe_2O_7$ in the paramagnetic phase.

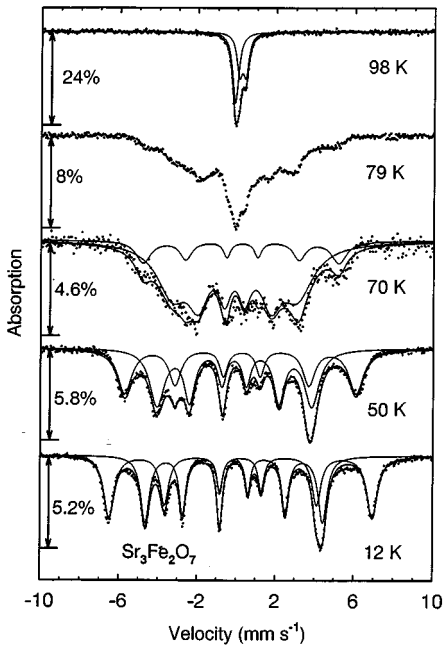

FIG. 2. Mössbauer spectra of $Sr_3Fe_2O_7$ in the magnetically ordered phase and in the temperature range of the phase transition.

The spectra between 12 and 70 K evidence magnetic ordering and have been analyzed by two hyperfine sextets. The intensity ratios between the different components of each hyperfine sextet were fixed to 3:2:1:1:2:3, and three linewidth parameters for each sextet were used for fitting the spectra. The resultant isomer shifts δ, magnetic hyperfine fields B_{hf}, and area fractions for sites I and II, as well as the quadrupole interaction parameter ε for site I, are given in Table 2. Site I is characterized by larger δ and B_{hf} values than site II. In agreement with previous Mössbauer studies on $Sr_3Fe_2O_7$ (3, 10) the intensity ratio of the two sites is found to be approximately 1:1 in the spectra at 20 and 12 K. However, the area fraction of the outer component I decreases with increasing temperatures as seen already from the 50-K spectrum and, in spite of the rather poor statistics, is clearly evident from the 70-K spectrum. The latter can still be analyzed by two hyperfine sextets although particularly the inner component is strongly broadened. The 79-K spectrum evidences the coexistence of paramagnetic and magnetically ordered sites, the fraction of the latter being dominant. On the other hand, the 98-K spectrum reveals signals due to paramagnetic ions only. Accordingly the transition to the magnetically ordered phase occurs in a rather narrow temperature range between

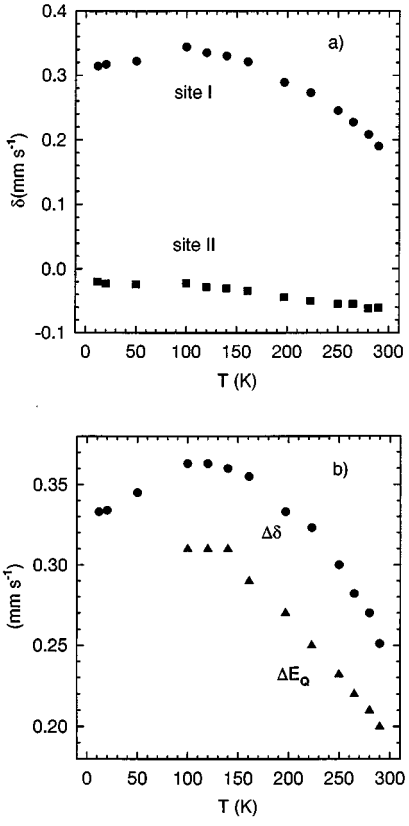

FIG. 3. Temperature dependence (a) of the isomer shifts of sites I and II and (b) of the quadrupole splitting ΔE_Q of site I and the difference $\Delta\delta$ in isomer shifts for $Sr_3Fe_2O_7$.

98 and 70 K, which seems to be somewhat lower than that in Ref. (3).

In Fig. 4 room temperature Mössbauer spectra of $Sr_{2.7}Ba_{0.3}Fe_2O_7$ and $Sr_{2.6}La_{0.4}Fe_2O_7$ are shown. The spectrum of the Ba-substituted material is very similar to that of

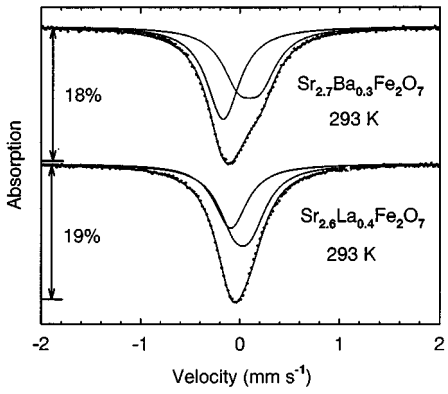

FIG. 4. Room temperature Mössbauer spectra of $Sr_{2.7}Ba_{0.3}Fe_2O_7$ and $Sr_{2.6}La_{0.4}Fe_2O_7$. The solid lines correspond to fits assuming a charge disproportionation of Fe^{4+}.

undoped $Sr_3Fe_2O_7$, whereas the spectrum of the La-substituted sample consists essentially of a single broad line. The spectrum of $Sr_{2.7}Ba_{0.3}Fe_2O_7$ has again been fitted assuming two sites with a fixed intensity ratio of 1 : 1. The single line in the spectrum of $Sr_{2.6}La_{0.4}Fe_2O_7$ is broadened and appears slightly asymmetric. There is no unique analysis for this spectrum. Guided by the possibility of a charge disproportionation of Fe^{4+}, the spectrum was reproduced by two sites with an intensity ratio of 3 : 2 (see below). The parameters are summarized in Table 3. The temperature dependence of the Mössbauer spectra of $Sr_{2.7}Ba_{0.3}Fe_2O_7$ and $Sr_{2.6}La_{0.4}Fe_2O_7$ is depicted in Figs. 5 and 6, respectively. It is evident that the 20-K spectra reveal two distinct sites with different isomer shifts δ and hyperfine fields B_{hf} (c.f. Table 3). The intensity ratios of the two sextets are in both cases 1 : 1. The lines are considerably broader than for $Sr_3Fe_2O_7$ which indicates a distribution of hyperfine fields due to structural disorder. For purposes of comparison it is

TABLE 2
Mössbauer Parameters of $Sr_3Fe_2O_7$

	T (K) →	12	20	50	70	120	293
Site I	δ	0.312(4)	0.315(5)	0.322(10)	0.33[a]	0.335(6)	0.190(1)
	ε rsp. ΔE_Q	− 0.03(1)	− 0.03(1)	− 0.04(1)	− 0.04[a]	0.31(1)	0.20(2)
	B_{hf}	41.59(3)	41.33(4)	36.59(8)	31.0(4)		
	Area (%)	51.7(8)	50.6(9)	44(2)	17(4)	50[a]	50[a]
Site II	δ	− 0.021(4)	− 0.019(4)	− 0.024(7)	− 0.02[a]	− 0.028(4)	− 0.061(6)
	B_{hf}	28.10(3)	27.83(4)	24.51(7)	19.8(3)		
	Area (%)	48.3(8)	49.4(9)	56(2)	83(4)		
	$\Delta\delta$	0.333	0.334	0.345	0.35[a]	0.363	0.251
	ΔB	13.49	13.50	12.08	11.2		

Note. ΔE_Q corresponds to the quadrupole splitting in the paramagnetic phase; ε is the quadrupole splitting parameter in the magnetically ordered phase. The units are mm s^{-1} for δ, ΔE_Q, and ε, and Tesla for B_{hf}.

[a] Parameter was not varied.

TABLE 3
Mössbauer Parameters of $Sr_{3-x}A_xFe_2O_7$

		$Sr_{2.7}Ba_{0.3}Fe_2O_7$		$Sr_{2.6}La_{0.4}Fe_2O_7$	
	T (K) →	293	20	293	20
Site I	δ	0.202(4)	0.339(10)	0.133(5)	0.344(7)
	ε rsp. ΔE_Q	0.219(8)	− 0.03(1)	0.17(2)	0.00(1)
	B_{hf}		40.72(8)		42.64(6)
	Area (%)	50[a]	48(2)	60[a]	50(1)
Site II	δ	− 0.061(3)	− 0.001(7)	0.015(9)	0.026(7)
	B_{hf}		27.31(6)		28.16(6)
	Area (%)	50[a]	52(2)	40[a]	50(1)
	$\Delta\delta$	0.263	0.338	0.118	0.318
	ΔB		13.41		14.48

Note. The units are mm s^{-1} for δ, ΔE_Q, and ε, and Tesla for B_{hf}.
[a] Parameter was not varied.

instructive to refer to the difference ΔB between the hyperfine fields at the two sites. It is realized that ΔB is nearly the same for $Sr_{2.7}Ba_{0.3}Fe_2O_7$ and $Sr_3Fe_2O_7$ whereas it is about 1 T larger for $Sr_{2.6}La_{0.4}Fe_2O_7$. The difference in isomer shifts $\Delta\delta$ for the latter compound is slightly smaller than for the other two materials. The development of magnetic order in the substituted samples has not been studied in detail, but it is seen from Fig. 5 that the 75-K spectrum of $Sr_{2.7}Ba_{0.3}Fe_2O_7$ is still characteristic of the paramagnetic phase whereas the 51-K spectrum reveals a broad magnetic hyperfine pattern. The 65-K spectrum of $Sr_{2.6}La_{0.4}Fe_2O_7$

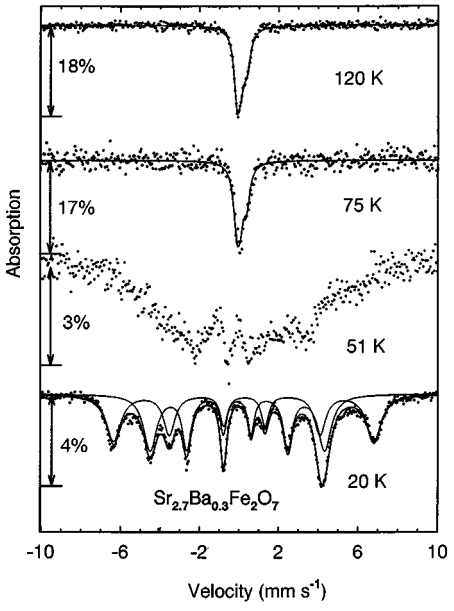

FIG. 5. Temperature dependence of the Mössbauer spectra of $Sr_{2.7}Ba_{0.3}Fe_2O_7$.

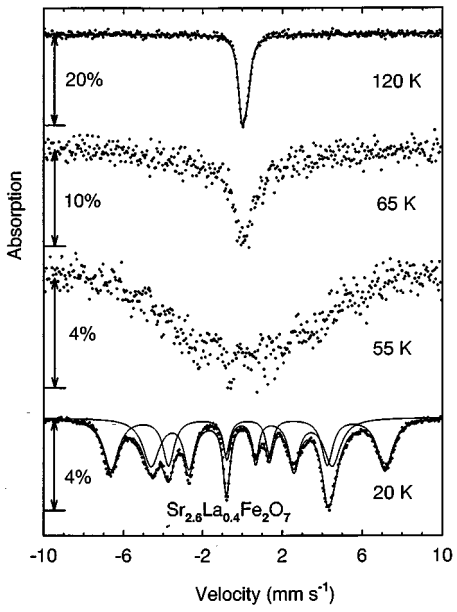

FIG. 6. Temperature dependence of the Mössbauer spectra of $Sr_{2.6}La_{0.4}Fe_2O_7$.

(Fig. 6) is dominated by the signal from paramagnetic ions but broad wings indicate the presence of a magnetic background. A magnetic hyperfine pattern is clearly developed in the 55-K spectrum.

The cationic substitutions have pronounced consequences for the magnetic behavior, as demonstrated in Fig. 7 where the inverse susceptibilities χ^{-1} are depicted as a function of temperature. The $\chi^{-1}(T)$ curves of $Sr_3Fe_2O_7$ and $Sr_{2.7}Ba_{0.3}Fe_2O_7$ reveal minima at about 110 and 60 K, respectively, which correspond to maxima in the $\chi(T)$ curves and indicate antiferromagnetic ordering. The $\chi(T)$

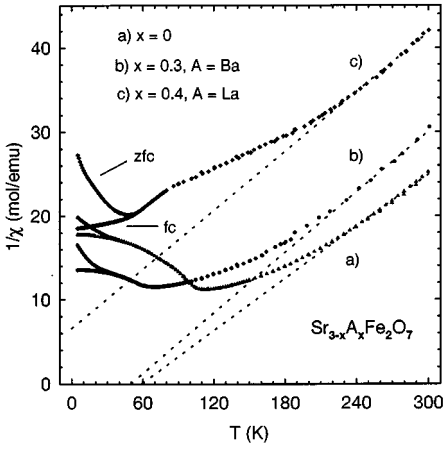

FIG. 7. Inverse magnetic susceptibilities as a function of temperature for $Sr_{3-x}A_xFe_2O_7$. The dotted lines correspond to fits assuming a Curie–Weiss law.

curve of $Sr_3Fe_2O_7$ compares reasonably well with previous susceptibility data of this compound (10, 20). There are no remarkable differences in the zfc and fc curves in the temperature range of the magnetic phase transition and above, but below 40 K the fc and zfc curves start to deviate. For the La-doped sample a broad minimum in $\chi^{-1}(T)$ is observed at about 50 K only in the zfc but not in the fc curve. At temperatures above 50 K zfc and fc curves agree well. The $\chi^{-1}(T)$ data for the paramagnetic phases deviate from a straight line which would be expected for Curie–Weiss law $\chi(T) = C/(T - \Theta)$. From a linear regression of the data between 220 and 300 K one obtains a positive value for Θ in the cases of $Sr_3Fe_2O_7$ and $Sr_{2.7}Ba_{0.3}Fe_2O_7$ but a negative value in $Sr_{2.6}$ $La_{0.4}Fe_2O_7$. The Θ parameters and the effective magnetic moments μ_{eff} calculated from the Curie constants are given in Table 4. The slopes of the $\chi^{-1}(T)$ curves decrease with decreasing temperature which corresponds to an increase in μ_{eff}. The magnetic ordering temperatures T_N are best derived from the temperature dependence of the derivatives $d(\chi T)/dT$ which reveal rather sharp cusps at 100 K for $Sr_3Fe_2O_7$ and at 57 K for $Sr_{2.7}Ba_{0.3}Fe_2O_7$. Only a broad maximum in the zfc but not in the fc curves of $d(\chi T)/dT$ is observed for $Sr_{2.6}La_{0.4}Fe_2O_7$, which indicates the absence of long-range magnetic order.

Also the electrical transport behavior is influenced by the cationic substitutions as seen from a plot of the logarithm of the conductivity $\sigma = 1/\rho$ versus inverse temperature (Fig. 8). All the compounds are semiconductors. Frequently σ follows an Arrhenius-type equation

$$\sigma(T) = A \exp(-E_\sigma/k_B T), \qquad [1]$$

where E_σ is the activation energy for the transport. It is apparent from the $\log \sigma$ vs $1/T$ data that the conductivities of the $Sr_{3-x}A_xFe_2O_7$ phases cannot be reproduced by Eq. [1]. In the cases of $Sr_3Fe_2O_7$ and $Sr_{2.7}Ba_{0.3}Fe_2O_7$ a certain low-temperature conductivity occurs which is only weakly activated. At higher temperatures a continuous crossover to more activated behavior is observed. The low-temperature conductivity of $Sr_{2.6}La_{0.4}Fe_2O_7$ is some orders

TABLE 4
Results from the Magnetic Susceptibility Data of $Sr_{3-x}A_xFe_2O_7$

Compound	μ_{eff} (μ_B)	Θ (K)	T_N (K)	T_m (K)
$Sr_3Fe_2O_7$	6.22	59	100	110
$Sr_{2.7}Ba_{0.3}Fe_2O_7$	5.78	50	57	60
$Sr_{2.6}La_{0.4}Fe_2O_7$	5.84	−56		50

Note. The magnetic ordering temperatures T_N were obtained from the cusps in the derivatives $d(\chi T)/dT$. T_m corresponds to the temperature of the maximum in the zfc-$\chi(T)$ curves. Magnetic moments μ_{eff} and Θ parameters were derived from a Curie–Weiss plot between 220 and 300 K.

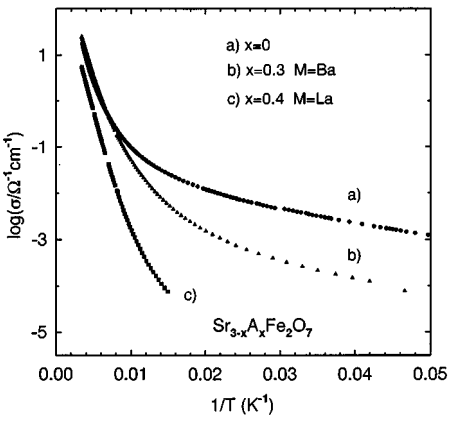

FIG. 8. Conductivities as a function of inverse temperature for $Sr_{3-x}A_xFe_2O_7$.

of magnitude smaller and could not be measured accurately with the present instrumentation. A regression of suitable linear parts of the $\log \sigma$ vs $1/T$ plots below room temperature yields E_σ values of 0.11 eV for $Sr_{2.7}Ba_{0.3}Fe_2O_7$ and 0.12 eV for $Sr_{2.6}La_{0.4}Fe_2O_7$. There is no well-defined linear part in the $\log \sigma$ vs $1/T$ plot of $Sr_3Fe_2O_7$.

The low-temperature conductivity of some mixed-valence transition metal oxides has been described by a Mott variable range hopping law

$$\sigma(T) = A \exp(-(T_0/T)^{1/4}). \qquad [2]$$

A plot of $\log \sigma$ vs $T^{-1/4}$ is essentially linear below 50 K for $Sr_3Fe_2O_7$ but the corresponding plot for $Sr_{2.7}Ba_{0.3}Fe_2O_7$ reveals still some curvature in the same temperature range.

4. DISCUSSION

4.1. Electronic Structure Considerations

For rationalizing the electronic behavior of strontium ferrates(IV) we consider a qualitative Mott–Hubbard-type picture of the electronic structure of transition metal compounds as described by Goodenough (21, 22). In the case of a single localized Fe^{4+} ion, which has an ideal octahedral environment of six oxygen atoms, the five 3*d* orbitals are split into t_{2g} and e_g subsets which, within a molecular orbital framework, are π^* and σ^* iron–oxygen antibonding orbitals, respectively. The covalency of iron–oxygen bonding may be described by mixing parameters $\lambda_i = b^i_{ca}/(E^i_d - E^i_p)$, where $i = \sigma$, π and $b^i_{ca} = \langle \Phi^i_c | H | \Phi^i_a \rangle$ are the transfer integrals accounting for the interaction between the cation and anion atomic orbitals Φ^i_c and Φ^i_a. In the case of the Fe^{4+} oxides the covalency is large as the energy difference $E_d - E_p$ between transition metal 3*d* and O 2*p* orbitals decreases from the left- to the right-hand side of the 3*d* series and with increasing oxidation state of a given transition

metal ion. The strong covalency of chemical bonding is confirmed by molecular orbital calculations (23) and by the analysis of photoelectron spectra of $SrFeO_3$ (24) which also evidence that Fe^{4+} is in a high-spin state. The electronic ground state of $3d^4$ high-spin ions like Cr^{2+}, Mn^{3+}, and Fe^{4+} in an octahedral ligand field is a Jahn–Teller active ^5E_g state which should give rise to structural distortions. However, the FeO_6 octahedra in $SrFeO_3$ are regular and the compound remains a cubic perovskite down to 4 K. Also the FeO_6 octahedra in the crystal structure of $Sr_3Fe_2O_7$, where the point symmetry at the iron sites is C_{4v}, are nearly regular. The iron–oxygen bond lengths in the xy planes (4×192.7 pm) are only slightly smaller than the apical ones (1×193.6 pm, 1×195.8 pm) (6). In the case of a localized $3d^4$ system this difference could result in a small splitting of the e_g orbitals into a_1 ($\sigma^*_{z^2}$) and b_1 ($\sigma^*_{x^2-y^2}$) orbitals which yields a $^5B_1$ electronic ground state for a single Fe^{4+} ion.

Within a Mott–Hubbard-type picture the electronic behavior of transition metal oxides is determined by a competition between the gain of kinetic energy by electron delocalization and the normally positive change in electron interaction energy U associated with charge fluctuations $\psi^n_\alpha + \psi^n_\beta \rightarrow \psi^{n-1}_\alpha + \psi^{n+1}_\beta$ between the metal–oxygen antibonding orbitals ψ on adjacent transition metal sites α and β which favors electron localization. The tendency for electron delocalization may be described by a transfer energy $b_i \propto \lambda_i^2$ $(i = \sigma, \pi)$. According to the classification of transition metal oxides proposed by Goodenough (21, 22) three main regions of electronic behavior may be distinguished. If b is smaller than a characteristic value b_c then the d electrons are localized and ligand-field theory is an adequate starting point for describing the electronic states. If, on the other hand, b is larger than a value b_m, a paramagnetic metal is found. For the intermediate regime $b_c < b < b_m$ collective correlated electronic states are formed the nature of which is determined by both the electron correlation and the tendency for electron delocalization.

The metallic-like conductivity in $SrFeO_3$ coexisting with magnetic order and the nearly regular FeO_6 octahedra suggest that the $Sr_{n+1}Fe_nO_{3n+1}$ series of strontium ferrates belongs to the intermediate region. Since $\lambda_\sigma > \lambda_\pi$, the π^* electrons may be assumed as localized, whereas the σ^* orbitals form narrow bands. Within the tight-binding approximation of band theory the transfer matrix elements b_σ give rise to bandwidth $w_\sigma \approx 2zb_\sigma$ of the σ^* band where z is the number of nearest-neighbor metal ions. Since z increases from $z = 4$ in Sr_2FeO_4 via $z = 5$ in $Sr_3Fe_2O_7$ to $z = 6$ in $SrFeO_3$, whereas the iron–oxygen bond lengths remain rather similar, it is essentially the ratio w_σ/U that is changed across the series. Accordingly, the strontium ferrates(IV) provide a good possibility for the characterization of the insulator–metal borderline region in a strongly correlated electronic system in more detail by tuning the electronic behavior from a more localized to a more delocalized regime. The 3 : 2 : 7 system, which is the subject of the present work, has an intermediate bandwidth within the series of strontium ferrates which suggests that the charge disproportionation of Fe^{4+} may occur for a certain range of transfer energies b_σ prior to the insulator–metal transition. In a similar way the difference between the electronic properties of $CaFeO_3$ and $SrFeO_3$ has been rationalized (25). In the tetragonally distorted crystal structure of $CaFeO_3$ the Fe–O–Fe bond angle is decreased from 180° which also yields a smaller w_σ and results in a charge disproportionation of Fe^{4+}.

The detailed description of electronic states in transition metal compounds is still a subject of intense research. Within an impurity-type framework of the electronic structure, oxoferrates(IV), similar to oxocuprates(III), are characterized by a negative effective M $3d$–O $2p$ charge-transfer energy which leads to a p–p-type excitation gap between insulating and metallic electronic states (26–28). It appears, however, questionable whether the neglect of the dispersion of the d states, which is inherent in impurity models, is justified for metal ions in high oxidation states.

4.2. Structural Data

The X-ray powder diagrams of $Sr_{2.7}Ba_{0.3}Fe_2O_7$ and $Sr_{2.6}La_{0.4}Fe_2O_7$ show that the tetragonal crystal structure of the parent compound is retained. Additional oxygen uptake occurs when the materials are annealed under high oxygen pressure as seen from the decrease in the lattice parameters a (see Table 1). By considering in addition the Mössbauer spectra discussed below it is concluded that the high-pressure annealed samples do not contain major oxygen deficiencies. This is in accord with preliminary neutron diffraction data of two samples of these phases which yield the compositions $Sr_{2.7}Ba_{0.3}Fe_2O_{6.95(1)}$ and $Sr_{2.6}La_{0.4}Fe_2O_{7.01(1)}$, respectively (29). Accordingly, the increase in the lattice constants a and c in samples where Sr^{2+} is substituted by isovalent Ba^{2+} just reflects the larger ionic radius of the latter. From the lattice constant a it is derived that the iron–oxygen distances in the iron–oxygen planes of $Sr_{2.7}Ba_{0.3}Fe_2O_7$ are 0.8 pm larger than those in $Sr_3Fe_2O_7$. Also, in the case of La-substitution both lattice parameters increase. Since La^{3+} is smaller than Sr^{2+} the dominant effect giving rise to the lattice expansion of $Sr_{2.6}La_{0.4}Fe_2O_7$ is the creation of larger Fe^{3+} instead of Fe^{4+} ions in the iron–oxygen network, which is required for conserving charge neutrality.

4.3. Mössbauer Spectra

Within the model of a charge disproportionation of Fe^{4+} into Fe^{3+} and Fe^{5+} one can assign component I in the Mössbauer spectra of $Sr_{3-x}A_xFe_2O_7$ to Fe^{3+} species and

component II to Fe^{5+} species. In fact, the differences $\Delta\delta$ of the isomer shifts and ΔB of the hyperfine fields between the two sites in $Sr_3Fe_2O_7$ and $Sr_{2.7}Ba_{0.3}Fe_2O_7$ are in good agreement with the corresponding values for $CaFeO_3$ ($\Delta\delta = 0.34\ mm\ s^{-1}$, $\Delta B = 13.7$ T) (13). Obviously the rather small weakening of the iron–oxygen bonds in $Sr_{2.7}Ba_{0.3}Fe_2O_7$, which is a consequence of the increased iron–oxygen bond lengths, has no influence on the charge disproportionation. On the other hand, the onset of magnetic ordering in the Mössbauer spectra of the Ba-substituted sample occurs at temperatures lower than that for $Sr_3Fe_2O_7$. This observation is in agreement with the magnetic susceptibility data and can be explained by a weakening of the magnetic exchange interactions in course of the lattice expansion.

With respect to a more complete understanding of the nature of the charge disproportionation state it is remarkable that the quadrupole splitting ΔE_Q of site I in the paramagnetic phase of $Sr_3Fe_2O_7$ (Fig. 3) is temperature dependent which is not expected for normal high-spin Fe^{3+}, where both σ^* orbitals are equally populated. Since in this case there is no valence contribution to the electric-field gradient tensor, there should only be a nearly temperature independent lattice contribution. A trend similar to that in ΔE_Q for site I is also observed for the difference $\Delta\delta$ of the isomer shifts. The temperature dependence of the isomer shifts usually arises from the second-order Doppler shift (SOD). Since such a large difference in the SOD for two sites in the same lattice appears unlikely, the temperature dependence of $\Delta\delta$ may rather indicate that the charge difference between the two sites in the paramagnetic phase is somewhat temperature dependent and increases with decreasing temperature. A temperature dependence of the quadrupole splitting may result if the electron accumulation at site I is accompanied by local structural rearrangements as oxygen displacements (c.f. anomalies in the temperature factors of the oxygen atoms in the neutron diffraction data of $Sr_3Fe_2O_7$ (10)), which are reduced with decreasing degree of charge disproportionation. On the other hand, the lack of a significant quadrupole splitting suggests that the local environment at the Fe^{5+}-like sites II is more symmetrical. A temperature dependence of the charge difference between the two sites, which is, however, much more pronounced and leads to an average-valence phase above 290 K, has been observed for $CaFeO_3$ (15).

The temperature dependence of the Mössbauer parameters supports an interpretation of the charge disproportionation in terms of a collective electronic state leading to fractional occupancies $1 + y$ and $1 - y$ of the σ^* orbitals at sites I and II, respectively. The concept of a gradual charge disproportionation was already invoked by Takano and Takeda to explain the continuous development of the Mössbauer spectra of $Ca_{1-x}Sr_xFeO_3$ and $Sr_{1-x}La_xFeO_3$ (14, 15). Presumably, the charge disproportionation of Fe^{4+} even in the magnetic phases of $CaFeO_3$ and $Sr_3Fe_2O_7$ is not complete either. This provides a natural explanation why the differences in isomer shifts and hyperfine fields between the two sites are much smaller than expected on the basis of data of comparable Fe^{3+} (c.f. $\delta(4\ K) = 0.47\ mm\ s^{-1}$, $B_{hf} = 56$ T for $LaFeO_3$ (16)) and Fe^{5+} (c.f. $\delta(4\ K) = -0.34\ mm\ s^{-1}$, $B_{hf} = 23$ T for La_2FeLiO_6 (30)) perovskite-type oxides. In addition, assuming a gradual charge disproportionation may also explain why structural modifications are smaller than expected for a complete charge disproportionation.

The La-substituted phase $Sr_{2.6}La_{0.4}Fe_2O_7$ formally contains 80% Fe^{4+} and 20% Fe^{3+}. It is readily seen from the low-temperature Mössbauer spectrum (Fig. 6) that the area fraction of the Fe^{3+}-like site I is much larger than 20%. From the fit of the 20-K spectrum one obtains an area ratio of 1 : 1 for the two sites. Obviously the charge disproportionation of Fe^{4+} is retained in the case of the valence-changing substitution of La^{3+} for Sr^{2+}. Isomer shift and hyperfine field values for site I are still considerably smaller than for typical oxoferrates(III) but B_{hf} is larger than for undoped $Sr_3Fe_2O_7$. The hyperfine field difference ΔB between the two sites, which is a measure for the difference in the density of unpaired spins, has increased by 1 T. In spite of some line broadening due to structural disorder one observes merely a single Fe^{3+}-like signal in the La-doped sample which indicates that a uniform collective electronic state is formed. Substitution of Sr^{2+} with La^{3+} corresponds to electron doping the 3 : 2 : 7 phase and leads to an increase in the average population of the σ^* orbitals at site I. This is the reason B_{hf} at site I increases into the direction of values which are typical for Fe^{3+} compounds. Similar effects can be seen in the Mössbauer data of several other mixed-valent oxoferrates(III, IV) (15–18, 31). There seems to be a continuous increase of B_{hf} at site I with increasing Fe^{3+} content. It is noteworthy that a charge disproportionation of Fe^{4+} has even been reported for phases with Fe^{4+} contents of only 10% in the series $Sr_{1-x}La_xFeO_3$ (16).

A certain discrepancy with respect to the model of a charge disproportionation seems to occur as the area fractions derived from the fit of the low-temperature spectrum of $Sr_{2.6}La_{0.4}Fe_2O_7$ reveal 50% component I and 50% component II instead of 60% and 40%, respectively. This result is found to be reproducible under different fitting constraints. It is seen, however, from the Mössbauer spectra of unsubstituted $Sr_3Fe_2O_7$ that the 1 : 1 area ratio of the two sextets is found only well below the magnetic ordering temperature (Fig. 2), whereas the area fraction of the outer component I is considerably reduced in the temperature range of the transition to the magnetically ordered state. This effect is particularly evident in the 70-K spectrum and is presumably a consequence of a relaxational collapse of the magnetic state. Also the broad magnetic pattern in the 79-K spectrum of $Sr_3Fe_2O_7$ is in favor of relaxational

behavior. Even in the 50-K spectrum of $Sr_3Fe_2O_7$, which appears already static, the area fraction of site I is only 44(2)%. Relaxation effects in the temperature range where magnetic order is developed are also clearly evident in the Mössbauer spectra of $Sr_{2.7}Ba_{0.3}Fe_2O_7$ and $Sr_{2.6}La_{0.4}Fe_2O_7$ (Figs. 5, 6). Considering that magnetic ordering effects in the spectra of $Sr_{2.6}La_{0.4}Fe_2O_7$ are only observed below 60 K and that the compound turns out to behave like a spin-glass (vide infra) it is possible that the area fractions at 20 K still underestimate the fraction of Fe^{3+}-like sites.

Finally, the question remains whether a charge disproportionation of Fe^{4+} also exists in the paramagnetic phase of $Sr_{2.6}La_{0.4}Fe_2O_7$ or whether an average-valence phase occurs which has been found in other formally mixed valence oxoferrates(III, IV) (17, 18). As there is no unique analysis for the Mössbauer spectra this question cannot be answered unambiguously. If one fits the spectra with fixed intensity ratios (see above) assuming a charge disproportionation of Fe^{4+} it is seen that $\Delta\delta$ and consequently any charge difference between the iron sites in the La-substituted material must be much smaller than for unsubstituted $Sr_3Fe_2O_7$ and for $Sr_{2.7}Ba_{0.3}Fe_2O_7$.

4.4. Magnetism

As discussed above the electronic ground state of Fe^{4+} in $Sr_3Fe_2O_7$ would be a $^5B_1$ state if the 3*d* electrons were localized. In this case the angular momentum contribution to the effective magnetic moment μ_{eff} should be quenched and one expects a spin-only moment of 4.9 μ_B per Fe^{4+} ion, in good agreement with the values of rather isolated Fe^{4+} in the ordered K_2NiF_4-type phases $(A, A')_2M_{0.5}Fe_{0.5}O_4$ (32, 33). The values of μ_{eff} derived from the $\chi^{-1}(T)$-curves of $Sr_3Fe_2O_7$ and $Sr_{2.7}Ba_{0.3}Fe_2O_7$ between 220 and 300 K are considerably larger than 4.9 μ_B, and in addition, the Θ values are positive. These results suggest that even above the magnetic ordering temperature T_N magnetic clusters are formed which are dominated by ferromagnetic exchange interactions and which order antiferromagnetically below T_N. Presumably the magnetic clusters grow in size with decreasing temperature which gives rise to the decreasing slope in $\chi^{-1}(T)$. Similar behavior was observed, e.g., for $BaLaNiRuO_6$ (34) where also ferromagnetic interactions are thought to be dominant above T_N. The smaller magnetic ordering temperature of $Sr_{2.7}Ba_{0.3}Fe_2O_7$ in comparison with $Sr_3Fe_2O_7$ is attributed to a weakening of the magnetic exchange interactions as a consequence of the increase in Fe–O–Fe distances.

The magnetic behavior of the 3:2:7 system is closely related to the magnetism of the perovskite $SrFeO_3$ (7) and of the K_2NiF_4-type phase Sr_2FeO_4 (9, 10). Magnetic susceptibility data reveal that these two compounds order antiferromagnetically too and show ferromagnetic correlations above T_N. The magnetism of oxoferrates(IV) is determined by a competition between ferromagnetic and antiferromagnetic exchange interactions. Antiferromagnetic coupling arises from superexchange interactions between the localized half-filled π^* orbitals. Since the σ^* electrons are discussed most reasonably in terms of collective electron behavior (see above) the ferromagnetic exchange contributions may be attributed to the tendency to delocalize the σ^* electrons in the solid. In a charge-fluctuation process the σ^* electrons are still coupled to the more localized π^* electrons by exchange interactions which favor a ferromagnetic alignment of spins at adjacent sites. Therefore the relevant charge fluctuation may be formulated as

$$2(\pi^*)^{\uparrow\uparrow\uparrow}(\sigma^*)^{\uparrow} \rightarrow (\pi^*)^{\uparrow\uparrow\uparrow}(\sigma^*)^{0} + (\pi^*)^{\uparrow\uparrow\uparrow}(\sigma^*)^{\uparrow\uparrow}. \qquad [3]$$

This is comparable to the double-exchange mechanism in mixed-valence transition metal oxides (35). The competition between antiferromagnetic and ferromagnetic interactions are the reason for the helical spin structure of $SrFeO_3$ (7). Also the complicated Mössbauer spectra of the magnetically ordered phase of Sr_2FeO_4 have been interpreted in terms of a helical spin arrangement (10).

The magnetic moment of 5.9 μ_B derived from the susceptibility data of $Sr_{2.6}La_{0.4}Fe_2O_7$ between 220 and 300 K is again larger than the value of 5.1 μ_B expected for 20% Fe^{3+} and 80% Fe^{4+}, but the Θ value is now negative and about 100 K smaller than for the unsubstituted sample. In a pure Fe^{3+} compound the antiferromagnetic exchange interactions between the half-filled σ^* orbitals are dominant and determine the magnetic behavior. Since the number of Fe^{3+}-like sites and the average population of the σ^* orbitals at these sites are larger in the charge disproportionation phase of $Sr_{2.6}La_{0.4}Fe_2O_7$ than that in $Sr_3Fe_2O_7$, antiferromagnetic exchange interactions become more important which is reflected in the more negative Θ value. At high temperatures the magnetic cluster formation seems still to be dominated by ferromagnetic correlations as suggested by the large value for μ_{eff}.

Below 50 K a divergence of the fc and zfc susceptibility curves of $Sr_{2.6}La_{0.4}Fe_2O_7$ is found. This behavior is reminiscent of a spin-glass and has been observed recently for a variety of mostly Fe^{3+}-containing perovskite-derived oxides. Examples include magnetically nondilute materials with competing exchange interactions like Sr_2FeRuO_6 (34) and Sr_3FeRuO_7 (36) as well as magnetically dilute materials like $SrAFeMO_6$ (A = Sr, Ca, Ba; M = Nb, Sn, Ta) (37–40). An example involving about 50% Fe^{4+} is the phase $Sr_2FeTiO_{5.81}$ (41). Since the topology in the perovskite lattice does not give rise to frustrated sites if only near-neighbor exchange interactions are considered, it is believed that also the next-near-neighbor interactions have to be taken into account for understanding the magnetic phenomena. The present $Sr_{2.6}La_{0.4}Fe_2O_7$ sample is a further example for a magnetically nondilute spin-glass.

Substitution of Sr^{2+} by La^{3+} and the concomitant generation of additional Fe^{3+}-like sites introduces disorder and perturbs the delicate balance between ferro- and antiferromagnetic exchange interactions in this class of compounds. The result is frustration which prevents the development of long-range magnetic order.

The behavior of unsubstituted $Sr_3Fe_2O_7$ and of $Sr_{2.7}Ba_{0.3}Fe_2O_7$, which both formally contain only Fe^{4+} (although slight oxygen-deficiency may lead to Fe^{3+} contributions of up to 5%), is remarkable as the fc and zfc curves diverge below 40 K, whereas they are in good agreement between 40 K and T_N. This is in contrast to the magnetic susceptibilities of the K_2NiF_4-type compound Sr_2FeO_4 where fc and zfc curves compare well also in the low-temperature range. Sr_2FeO_4 does not show a charge disproportionation of Fe^{4+}. The different magnetic behavior of the 3:2:7 system is presumably related to additional exchange interactions which are a consequence of the higher degree of condensation of the iron–oxygen network in the crystal structure. The basic structural motifs are sheets of double octahedra, which can be considered as two coupled magnetic monolayers (42). Since in $Sr_3Fe_2O_7$ the Fe–O(1) distances within the layers are about 3 pm smaller than the apical Fe–O(3) distances, where O(3) atoms interconnect the two layers, it is likely that the exchange interactions in the iron–oxygen planes of a layer are somewhat stronger than those between the layers. Accordingly, the magnetic structure developing at T_N may be modified at lower temperatures when the exchange interactions between the layers become more important. Considering the competition between ferro- and antiferromagnetic exchange pathways it is suspected that slightly different spin orientations (e.g., angles between adjacent spins) in the magnetic phases may be the origin of the divergence of fc and zfc curves at low temperatures.

4.5. Electrical Transport Behavior

The temperature dependence of the conductivity σ of semiconductors reflects the creation of charge carriers (holes and electrons) by thermal excitation from the ground state into excited states as well as the temperature dependence of their mobility. It has been shown above (c.f. Fig. 8) that the $\log\sigma$ vs $1/T$ curves do not follow an Arrhenius equation but are characterized by a change from weakly activated low-temperature behavior to stronger activated high-temperature behavior. The low-temperature conductivities of $Sr_3Fe_2O_7$ ($\sigma \sim 10^{-2}$–$10^{-4}\,\Omega^{-1}\,cm^{-1}$ between 50 and 10 K) are intermediate within the series $Sr_{n+1}Fe_nO_{3n+1}$ of strontium ferrates(IV) (28). Non-Arrhenius behavior is also indicated by the conductivity data of Sr_2FeO_4 (9) but the low-temperature conductivities are too small to be measured accurately. On the other hand, the conductivities of stoichiometric $SrFeO_3$ are temperature-independent between 4 and 300 K with $\sigma \sim 10^3\,\Omega^{-1}\,cm^{-1}$ (5). Thus the low-temperature conductivities of the three compounds span a range of more than ten orders of magnitude which is in agreement with the view that the electronic structure parameters are in a critical range where the change from localized to itinerant electron behavior occurs. Within the Mott–Hubbard-type picture of the electronic structure sketched in Section 4.1 it is essentially the ratio w_σ/U and consequently the tendency to delocalize the σ^* electrons which is changed. The transition from localized to itinerant electron behavior seems to proceed in a gradual way. This is also suggested by the observation of a continuous increase in the near-infrared reflectivity of Sr_2FeO_4 at pressures above 5 GPa (11) which has been interpreted in terms of a gap narrowing, finally resulting in an insulator–metal transition. A deeper understanding of the electron transport mechanism in oxoferrates(IV) and its temperature dependence requires a more quantitative model of the electronic structure of these compounds. In addition, electron–phonon interactions may be involved in the transport process and lead to polaron formation.

The smaller low-temperature conductivity of $Sr_{2.7}Ba_{0.3}Fe_2O_7$ in comparison with the unsubstituted phase is attributed to a certain weakening of the transfer energy b_σ as a consequence of the increased Fe–O–Fe distances. La-substitution of the 3:2:7 phase, which introduces additional electrons, does not lead to metallic behavior. On the contrary, the low-temperature conductivity of $Sr_{2.6}La_{0.4}Fe_2O_7$ is some orders of magnitude smaller than for unsubstituted $Sr_3Fe_2O_7$ and for $Sr_{2.7}Ba_{0.3}Fe_2O_7$. Above 160 K the data can be described by an Arrhenius equation. The stronger localization of the electrons in the La-substituted phase may reflect a decrease of b_σ with increasing Fe^{3+} content as the energy difference between Fe 3*d* and O 2*p* orbitals for Fe^{3+} is larger than for Fe^{4+}.

Finally, it should be noted that all conductivity data available for the strontium ferrates have been measured on annealed powder pellets. Resistivity measurements on single crystals are desirable as the conductivities of the layered 2:1:4 and 3:2:7 phases are certainly anisotropic with larger conductivities within the iron–oxygen layers than along the *c* direction.

5. CONCLUSIONS

The present ^{57}Fe-Mössbauer studies on the iron(IV) phases $Sr_3Fe_2O_7$ and $Sr_{2.7}Ba_{0.3}Fe_2O_7$ and on the mixed-valence phase $Sr_{2.6}La_{0.4}Fe_2O_7$ evidence a charge disproportionation of Fe^{4+} in the magnetically ordered phases of all the compounds. In the paramagnetic phases of the two Fe^{4+} compounds a charge disproportionation is observed too, whereas the spectra of $Sr_{2.6}La_{0.4}Fe_2O_7$ indicate essentially an average-valence state. Magnetic susceptibility data of $Sr_3Fe_2O_7$ and $Sr_{2.7}Ba_{0.3}Fe_2O_7$ reveal antiferromagnetic

ordering below 100 and 57 K, respectively, but suggest the formation of a spin-glass below 50 K in $Sr_{2.6}La_{0.4}Fe_2O_7$. The magnetic behavior of the compounds is in favor of a competition of ferro- and antiferromagnetic exchange interactions. All three compounds are semiconductors, but the temperature dependence of the conductivities deviates from an Arrhenius equation.

The diversity of electronic phenomena in oxoferrates(IV) is most likely a consequence of an electronic situation where both a pronounced tendency to delocalize the σ^* electrons and strong on-site Coulomb and exchange interactions between the *d* electrons determine the nature of electronic states. For a certain range of values of the interaction energies the formation of a collective charge-disproportionation state, e.g., a charge-density wave, may be energetically most favorable for the system. The role of electron–lattice interactions for the stabilization of the charge disproportionation still remains to be clarified.

ACKNOWLEDGMENTS

I thank Dr. S. Eriksson and Dr. C. Ström (University of Göteborg) for their collaboration in exploring the chemistry of the substituted 3:2:7 system and for performing neutron diffraction studies on two samples, E. Brücher for performing the magnetic susceptibility measurements, N. Rollbühler for the resistivity measurements, and W. Hölle for assistance with sample preparation and characterization. Special thanks are to Professor P. Gütlich, University of Mainz, for the possibility of measuring low-temperature Mössbauer spectra in his laboratory and to several members of his group, in particular Dr. J. Jung, for their support and hospitality. Furthermore, I am indebted to Dr. R. K. Kremer for helpful discussions, to Professor A. Simon for his support, and to the Deutsche Forschungsgemeinschaft for a scholarship.

REFERENCES

1. R. Scholder, H. v. Bunsen, and W. Zeiss, *Z. Anorg. Allg. Chem.* **283,** 330 (1956).
2. C. Brissi, *Ann. Chim.* (*Rome*) **51,** 1399 (1961).
3. P. K. Gallagher, J. B. MacChesney, and D. N. E. Buchanan, *J. Chem. Phys.* **45,** 2466 (1966).
4. R. Scholder, F. Kindervater, and W. Zeiss, *Z. Anorg. Allg. Chem.* **283,** 338 (1956).
5. J. B. MacChesney, R. C. Sherwood, and J. F. Potter, *J. Chem. Phys.* **43,** 1907 (1965).
6. S. E. Dann, M. T. Weller, and D. B. Currie, *J. Solid State Chem.* **97,** 179 (1992).
7. T. Takeda, Y. Yamaguchi, and H. Watanabe, *J. Phys. Soc. Jpn.* **33,** 967 (1972).
8. P. K. Gallagher, J. B. MacChesney, and D. N. E. Buchanan, *J. Chem. Phys.* **41,** 2429 (1964).
9. P. Adler, *J. Solid State Chem.* **108,** 275 (1994).
10. S. E. Dann, M. T. Weller, D. B. Currie, M. F. Thomas, and A. D. Al-Rawwas, *J. Mater. Chem.* **3,** 1231 (1993).
11. P. Adler, A. F. Goncharov, K. Syassen, and E. Schönherr, *Phys. Rev. B* **50,** 11396 (1994).
12. G. R. Hearne, M. P. Pasternak, and R. D. Taylor, *Nuovo Cimento* **18,** 145 (1996).
13. M. Takano, N. Nakanishi, Y. Takeda, S. Naka, and T. Takada, *Mater. Res. Bull.* **12,** 923 (1977).
14. M. Takano, J. Kawachi, N. Nakanishi, and Y. Takeda, *J. Solid State Chem.* **39,** 75 (1981).
15. M. Takano and Y. Takeda, *Bull. Inst. Chem. Res. Kyoto Univ.* **61,** 406 (1983).
16. S. E. Dann, D. B. Currie, M. T. Weller, M. F. Thomas, and A. D. Al-Rawwas, *J. Solid State Chem.* **109,** 134 (1994).
17. T. C. Gibb and M. Matsuo, *J. Solid State Chem.* **81,** 83 (1989).
18. P. D. Battle, T. C. Gibb, and S. Nixon, *J. Solid State Chem.* **77,** 124 (1988).
19. P. D. Battle, T. C. Gibb, and P. Lightfoot, *J. Solid State Chem.* **84,** 271 (1990).
20. J. B. MacChesney, H. J. Williams, R. C. Sherwood, and J. F. Potter, *Mater. Res. Bull.* **1,** 113 (1966).
21. J. B. Goodenough and J. M. Longo, *in* "Magnetic and Other Properties of Oxides" (K.-H. Hellwege Ed.), Landoldt-Bornstein New Series III, Vol. 4, Springer-Verlag, Berlin (1970).
22. J. B. Goodenough, *Prog. Solid State Chem.* **5,** 145 (1971).
23. H. Adachi and M. Takano, *J. Solid State Chem.* **93,** 556 (1991).
24. A. E. Bocquet, A. Fujimori, T. Mizokawa, T. Saitoh, H. Namatame, S. Suga, N. Kimizuka, Y. Takeda, and M. Takano, *Phys. Rev. B* **45,** 1561 (1992).
25. M. Takano, S. Nasu, T. Abe, K. Yamamoto, S. Endo, Y. Takeda, and J. B. Goodenough, *Phys. Rev. Lett.* **67,** 3267 (1991).
26. T. Mizokawa, H. Namatame, A. Fujimori, K. Akeyama, H. Kondoh, H. Kuroda, and N. Kosugi, *Phys. Rev. Lett.* **67,** 1638 (1991).
27. T. Mizokawa, A. Fujimori, H. Namatame, K. Akeyama, and N. Kosugi, *Phys. Rev. B* **49,** 7193 (1994).
28. P. Adler, A. F. Goncharov, and K. Syassen, *Hyp. Int.* **95,** 71 (1995).
29. S. Eriksson, C. Ström, and P. Adler, unpublished results.
30. G. Demazeau, B. Buffat, F. Ménil, L. Fournés, M. Pouchard, J. M. Dance, P. Fabritchnyi, and P. Hagenmuller, *Mater. Res. Bull.* **16,** 1465 (1981).
31. M. Takano, T. Okita, N. Nakayama, Y. Bando, Y. Takeda, O. Yamamoto, and J. B. Goodenough, *J. Solid State Chem.* **73,** 140 (1983).
32. G. Demazeau, N. Chevreau, L. Fournes, J.-L. Soubeyroux, Y. Takeda, M. Thomas, and M. Pouchard, *Rev. Chim. Miner.* **20,** 155 (1983).
33. G. Demazaeu, Z. Li-Ming, L. Fournes, M. Pouchard, and P. Hagenmuller, *J. Solid State Chem.* **72,** 31 (1988).
34. P. D. Battle, T. C. Gibb, C. W. Jones, and F. Studer, *J. Solid State Chem.* **78,** 281 (1989).
35. C. Zener, *Phys. Rev.* **82,** 403 (1951).
36. P. D. Battle, S. K. Bollen, and A. V. Powell, *J. Solid State Chem.* **99,** 267 (1992).
37. T. C. Gibb, *J. Mater. Chem.* **3,** 441 (1993).
38. T. C. Gibb and R. J. Whitehead, *J. Mater. Chem.* **3,** 591 (1993).
39. T. C. Gibb, A. J. Herod, and N. Peng, *J. Mater. Chem.* **5,** 91 (1995).
40. P. D. Battle, T. C. Gibb, A. J. Herod, S.-H. Kim, and P. H. Munns, *J. Mater. Chem.* **5,** 865 (1995).
41. T. C. Gibb, P. D. Battle, S. K. Bollen, and R. J. Whitehead, *J. Mater. Chem.* **2,** 111 (1992).
42. R. Navarro, J. J. Smit, L. J. de Jongh, W. J. Crama, and D. J. W. Ijdo, *Physica B* **83,** 97 (1976).